W.-T. Hsu, J. R. Clark, and C. T.-C. Nguyen, “A sub-micron capacitive gap process for multiple-metal-electrode lateral micromechanical resonators,”, *Technical Digest*, IEEE Int. Micro Electro Mechanical Systems Conf., Interlaken, Switzerland, Jan. 21-25, 2001, pp. 349-352.

A SUB-MICRON CAPACITIVE GAP PROCESS FOR MULTIPLE-METAL-ELECTRODE LATERAL MICROMECHANICAL RESONATORS

Wan-Thai Hsu, John R. Clark, and Clark T.-C. Nguyen
Center for Wireless Integrated Microsystems
Department of Electrical Engineering and Computer Science
University of Michigan
Ann Arbor, Michigan 48109-2122

ABSTRACT

A fabrication process has been demonstrated that combines polysilicon surface micromachining, metal electroplating, and a sidewall sacrificial-spacer technique, to achieve high-aspect-ratio, submicron, *lateral* capacitive gaps between a micromechanical structure and its *metal* electrodes, without the need for advanced lithographic and etching technology. Among the devices demonstrated using this process are lateral free-free beam micromechanical resonators (Q=10,470 at 10.47 MHz), contour mode disk resonators (Q =9,400 at 156 MHz), and temperature-compensated micromechanical resonators (Q=10,317 at 13.5 MHz, with a −200ppm frequency variation over a full 80°C range).

I. INTRODUCTION

Vibrating micromechanical (or “µmechanical”) structures constructed in a variety of materials, from polycrystalline silicon to plated-nickel, have recently emerged as potential candidates for use in a myriad of frequency-selective communications applications [1]. To date, the majority of resonator demonstrations at VHF frequencies have utilized capacitive transduction, mainly for simplicity and ease of fabrication, especially when merging MEMS and IC transistor technologies [2]. For such devices, however, as dimensions are scaled to allow higher frequencies, the capacitive transducer gaps must also be scaled so that the electromechanical coupling can keep up with rising resonator stiffnesses; e.g., to insure an adequately small series motional resistance R_x for the device (c.f., Fig. 1). As a consequence, for VHF and above frequencies, capacitive transducer gaps of less than 1,000Å are required [3]. To date, this gap requirement has constrained capacitively-transduced resonators to operate in vertical modes (i.e., with displacements perpendicular to the substrate), since 1000Å gaps are much easier to achieve via film thickness control than by lithographic and etch control, which would be required for lateral mode devices (i.e., with displacements parallel to the substrate).

The inability to utilize lateral operation modes constitutes a serious limitation on the design space available for capacitively-transduced VHF resonators. Indeed, if lateral modes were available, then: (1) a wider variety of resonant vibration modes could be used, such as disk contour modes capable of more easily achieving higher frequency than flexural-mode counterparts; (2) balanced resonator geometries would be encouraged, such as tuning forks, which are well known to achieve higher Q than unbalanced designs, but which are more difficult to realize if constrained to vertical motion; and (3) the flexibility with which electrodes can be placed around a resonator structure would be greatly increased, making control and biasing schemes for MEMS devices much simpler [4].

This paper details a new fabrication process that combines polysilicon surface-micromachining, metal electroplating, and a sidewall sacrificial-spacer technique, to realize the cross-section shown in Fig. 2, where high-aspect-ratio, sub-micron, *lateral* capacitive gaps have been achieved between a µmechanical structure and its *metal* electrodes, without the need for advanced lithographic and etching technology. In addition to making possible all of the benefits listed above, this process also allows the simultaneous use of a

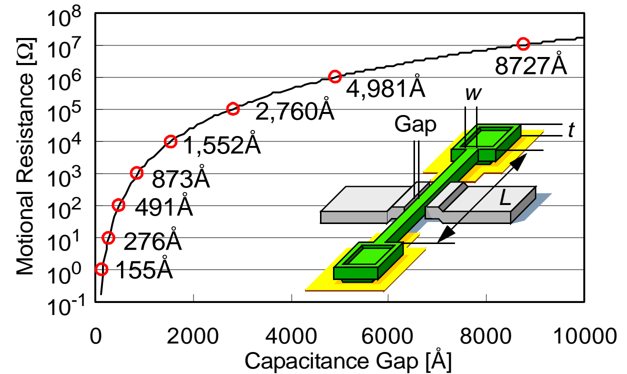

Fig. 1: Simulated plot of motional resistance versus electrode-to-resonator gap for a 40µm-long, 2µm-wide, 3µm-thick, lateral clamped-clamped beam µmechanical resonator.

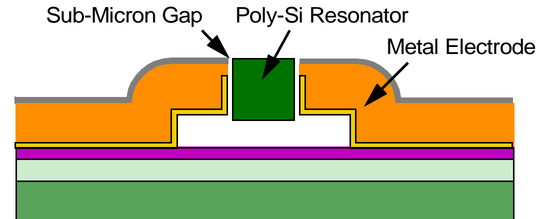

Fig. 2: Cross-section of the described sub-µm electrode-to-resonator gap process for lateral µstructures with metal electrodes.

high-Q structural material (e.g., polysilicon) together with highly conductive (i.e., low-loss) *metal* electrodes—an essential feature if µmechanical resonators are to reach GHz frequencies with sufficient Q and power handling ability. Using this process, a variety of new resonator devices have been demonstrated, including a 10.47 MHz lateral free-free beam resonator with Q >10,000, a 156 MHz contour-mode disk resonator with Q >9,000, and a 13.5 MHz temperature-compensated resonator with a −200ppm frequency variation over an 80°C range.

II. THE SUB-µm LATERAL CAPACITIVE GAP FABRICATION PROCESS

Figure 3 presents cross-sections and associated scanning electron micrographs (SEM’s) summarizing the process sequence of this work. As shown, the process begins with steps similar to those used in polysilicon surface micromachining to achieve the cross-section of Fig. 3(a). Specifically, a 2µm-thick oxide film is first thermally grown on the silicon substrate, followed by a 3000Å-thick film of LPCVD stoichiometric silicon nitride, and these two layers together serve to isolate devices and interconnects from the conductive silicon substrate. Interconnect polysilicon is then deposited via LPCVD to a thickness of 3000Å and doped via ion-implantation of phosphorous with an implantation energy of 60keV and a dose of 2×10^{16} cm^{-2}. After patterning this polysilicon to form ground planes and interconnects, 6000Å of LPCVD high-temperature oxide (HTO) is deposited at 920°C using a $SiCl_2H_4/N_2O$-based

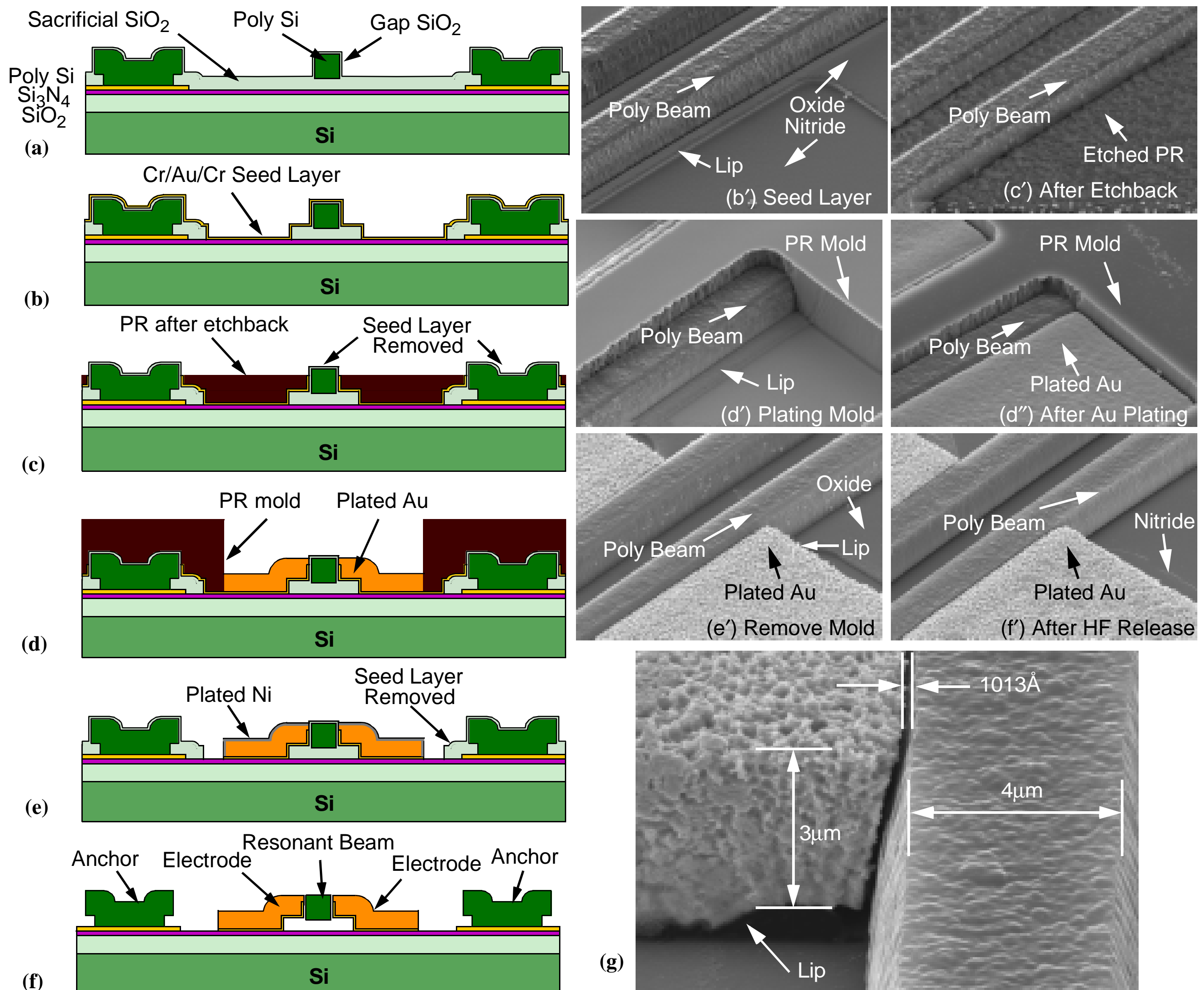

Fig. 3: Process flow for the multiple-metal-electrode, sub-μm gap, polysilicon lateral μresonator technology. (a)-(f) comprise cross-sectional diagrams of this process, while (b′)-(f′) and (g) present SEM's at different stages of the process.

recipe to serve as a sacrificial layer that temporarily supports the structural polysilicon layer during its own deposition and patterning. Before depositing the structural polysilicon, vias are first patterned and etched into this sacrificial layer to form anchors for the eventual structures. The structural polysilicon film is then deposited 2 to 4μm-thick via LPCVD at 588°C—the temperature needed to achieve a low-stress, fine-grained material. This film is doped via phosphorous implantation, then capped with a 3000Å-thick film of HTO that serves as both a hard mask during etching of the structural polysilicon, and as spacer layer during an electrode plating step to occur later in the process. Before etching, the structural polysilicon is annealed in N_2 at 1100°C for 1 hour to activate dopants and relieve residual stress—an important step in the process that insures a high Q structural material.

Next, the oxide hard mask is patterned and plasma etched to the desired device geometries, and these patterns are then transferred to the underlying structural polysilicon layer via a high density plasma RIE process, using a Cl_2/HBr chemistry to insure vertical sidewalls. At this point, the process deviates from standard surface micromachining: Instead of releasing structures, as would be done in a standard surface micromachining process, the process continues with the conformal deposition of 1000Å of HTO along the tops and sidewalls of the patterned polysilicon structures to serve as a sacrificial spacer layer that defines the eventual electrode-to-structure capacitive gap spacing. At this point, the process cross-section is as in Fig. 3(a). The bottom 6000Å sacrificial oxide is then patterned and etched via a combination of RIE and wet chemicals to expose the underlying nitride film (without attacking it) in areas where metal electrodes are to be formed.

In preparation for metal electroplating, a thin Cr/Au/Cr (200Å/300Å/200Å) film is evaporated over all areas (c.f., Fig. 1(b)(b′)) to serve as a seed layer. Next, a 40μm-thick layer of SJR5740 photoresist (PR) is spun on the wafer—thick enough to achieve a planarized surface, with the structural polysilicon topography deep under the PR film. The PR is then etched back using an O_2 plasma process until the seed layer over the tops of the polysilicon structures is exposed. The exposed top-level seed layer is then removed using a CR14/GE8148/CR14 solution to prevent metal from plating over the tops of the polysilicon structures during subsequent electrode plating steps. At this point, the cross-section is as in

Fig. 3(c)(c′). After removing the remaining film of SJR5740 photoresist, a 6μm-thick AZ9245 photoresist layer is applied and patterned to electrode geometrical specifications to form a mold that, together with the sidewall sacrificial oxide, defines the electrode plating boundaries.

Two metals were investigated as plated electrode materials: Ni and Au. Ni was originally expected to be the better of the two, since Ni sulfamate used for Ni plating is less corrosive to AZ9245 PR than the cyanide-based Au plating solution (which cracks AZ9245 PR after 15 min of exposure) first used. This allows for slower Ni plating rates, hence, more uniform Ni films. Unfortunately, however, plated Ni was found to have a finite etch rate in the concentrated HF solution used during a later structural release step. As a consequence, if Ni is used as the electrode material, the achievable electrode-to-resonator gap depends on the time needed to release structures in HF. This, combined with the discovery of a non-acid-based Au plating solution that did not corrode AZ9245 PR (even if not hard-baked), eventually led to a preference for Au electrodes.

Continuing with the process flow, after removing the top Cr layer to expose the Au seed layer (using the mold as a mask), Au is electroplated to form the electrodes and achieve the cross-section of Fig. 3(d) and the SEM of Fig. 3(d′). Au is plated until the electrode top is nearly flush with the top of the polysilicon structure, as shown in Fig. 3(d″). Note that the 3000Å-thick oxide layer on top of the polysilicon structures (originally used as a hard mask during poly etching) provides a buffer zone over which the electrode metal can be plated beyond the polysilicon thickness while still avoiding plating over the tops of the polysilicon structures. After plating, the photoresist mold is then removed, and a thin layer of Ni is plated over exposed Au electrode regions (with Cr blocking any plating in field regions) to protect them during a subsequent seed layer removal step (c.f., Fig. 3(e)(e′)). Seed layer removal is done using a $CH_3COOH/Ce(NH_4)_2(NO_3)_6$-based CR14 chrome etchant together with a KI-I_2/complex-phosphate-based GE8148 Au etchant. GE8148 is preferred over the more popular Type TFA Au etchant for this step, because the former does not etch plated Ni.

At last, structures are released in 49% concentrated HF to yield the final cross-section shown in Fig. 3(f)(f′). During the typical 20 min HF dip required to release all structures, the adhesion between Au electrodes and the nitride isolation layer remains intact. As shown in Fig. 3(g), the electrode-to-structure gap spacing is about 1013Å for the process run of this work—an aspect ratio of about 30 for the 3μm-thick structures depicted in the figure. Note that the aspect ratio is limited only by the conformability of HTO and the maximum thickness to which Au can be plated.

III. DEVICE DEMONSTRATIONS

To illustrate the benefits of this new lateral sub-μm-gap process technology, several lateral mode resonator devices are now described, each with significant performance enhancements over previous vertical mode counterparts.

Lateral Free-Free Beam μMechanical Resonator.

Figure 4(a) presents the SEM of a 10.47 MHz lateral free-free beam ("FF-beam") μmechanical resonator fabricated via the described process. This lateral FF-beam is similar to its vertical-mode counterpart [3] in that it utilizes an anchor-isolating suspension structure to suppress energy losses to the substrate at its resonance frequency. Unlike the vertical version, however, the support beams in this lateral device do not move in torsion; rather, they exhibit flexural-mode movements during resonance, and so must be designed such that they present a zero flexural mode impedance to the FF-beam during resonance vibration. This is done for the structure in Fig. 4(a) by attaching the support beams to nodal points on the FF-beam, recognizing that each set of two supports on opposite

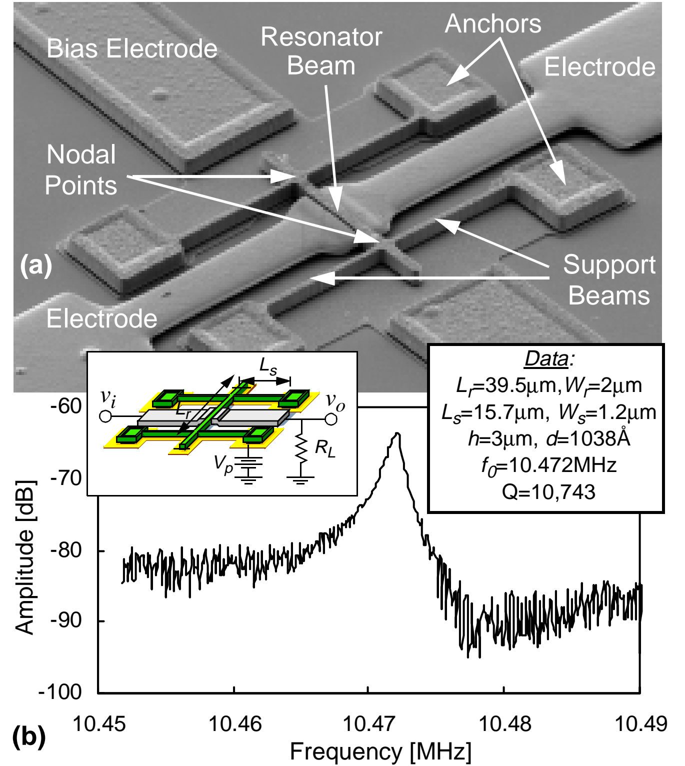

Fig. 4: (a) SEM of a fabricated lateral free-free beam μmechanical resonator (b) Measured frequency spectrum for the resonator (The inset shows the measurement set-up.)

sides of the FF-beam combine to form a clamped-clamped beam ("CC-beam") from anchor-to-anchor, then designing the dimensions of the supports so that their composite CC-beam resonates in a second mode when the FF-beam vibrates in its fundamental mode. In this scheme, the beam attachment locations correspond to nodal locations for both the FF-beam and the second mode composite CC-beams, and this insures minimal energy transfer between the two, hence, minimal energy loss, and maximum *Q*.

One clear advantage that the lateral FF-beam of Fig. 4(a) has over vertical-mode counterparts is its use of two electrodes, i.e., two ports. The availability of two-ports greatly simplifies the measurement of resonator frequency spectra, since parasitic feedthrough currents can be substantially suppressed if the second electrode is used as a sense port. In fact, the measured frequency characteristic in Fig. 4(b) not only exhibits a Q=10,743—one of the highest to date for ~10 MHz flexural-mode μmechanical resonators—but also lacks the distinct parallel resonant peak commonly seen in vertical resonator devices due to parasitic feedthrough [5].

Radial Contour-Mode Disk μMechanical Resonator.

Figure 5 presents the SEM of a 156 MHz VHF contour-mode, disk μmechanical resonator [6] with a 34μm diameter, fabricated via the described process. This device consists of a disk suspended 6,000Å above the substrate with a single anchor at its center. As shown, two plated-metal split electrodes surround the disk in order to allow routing to the structure while maintaining a symmetric distribution of force when electrostatically exciting the device. Given the very large stiffness of this device when operating in a radial contour mode (which allows it to achieve such high frequency), sub-μm lateral electrode-to-resonator gaps are essential for adequate transduction, and are conveniently provided via the described process. The symmetrical placement of electrodes, together with a fully balanced design that achieves a nodal point at the support

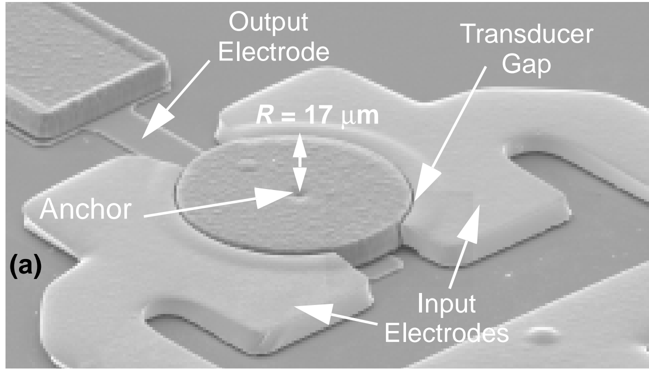

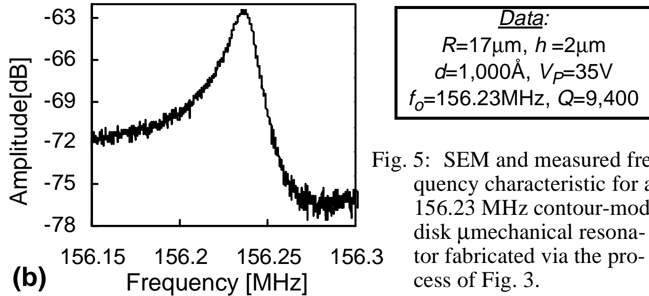

Fig. 5: SEM and measured frequency characteristic for a 156.23 MHz contour-mode disk μmechanical resonator fabricated via the process of Fig. 3.

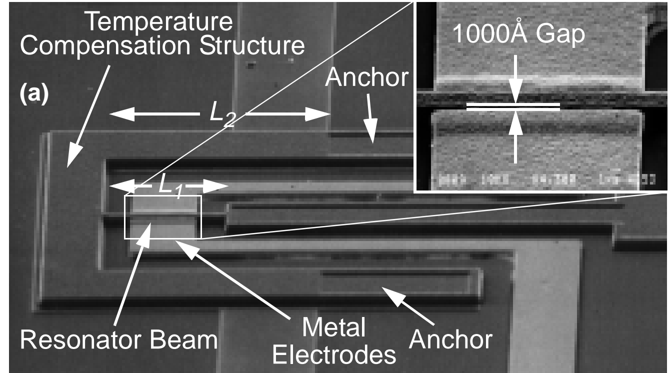

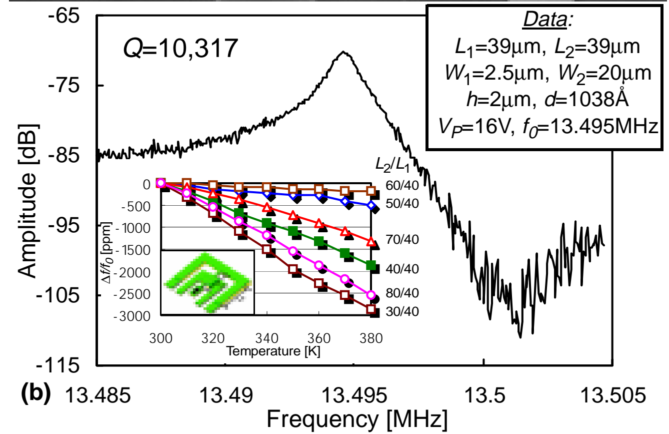

Fig. 6: (a) SEM of a temperature-insensitive micromechanical resonator fabricated using the process of Fig. 3. (b) Measured frequency characteristic and plot of fractional frequency change versus temperature for various beam ratios.

location of the disk, again made possible via the described process, allows this device to exhibit a very high Q even at mid-VHF frequencies. From the measured frequency characteristic in Fig. 5(b), the 156 MHz device of Fig. 5(a) shows a Q=9,400—the highest demonstrated to date at VHF frequencies for a on-chip resonator.

Geometric-Stress Temperature-Compensated μResonator.

Figure 4 presents the SEM of a 13.5 MHz geometric-stress temperature-compensated resonator [7], indicating key components and specifying the small gap in the inset. As shown, this structure consists of a flexural-mode resonator beam anchored to the substrate at one end, but supported on the other by a folded structure comprised of a truss section attached to two outer beams. Metal electrodes are positioned on either side of the resonator beam to allow lateral excitation. To insure that only the resonator beam vibrates when excitation signals are applied, the outer support beams are made much wider than the resonator beam, making them rigid against lateral motions. The outer beams are also designed to be longer than the resonator beam, so they will expand faster than it with increasing temperature, generating a net tension in the resonator beam. This tensile stress serves to increase the beam's resonance frequency, and thus, oppose frequency decreases caused by Young's modulus temperature dependence, resulting in a smaller overall resonance frequency excursion over a given temperature range.

Figure 4(b) shows the measured frequency characteristic for the device of (a), showing a very good Q=10,317. The inset presents a measured plot of fractional frequency change versus temperature for such resonators with various compensation ratios, showing a temperature coefficient of only −2.5ppm/^{o}C when L_2/L_1=60/40—the lowest yet achieved for a μmechanical resonator, and all made possible via the described sub-μm lateral gap process.

IV. CONCLUSIONS

A fabrication process capable of achieving sub-μm lateral gaps between polysilicon structures and metal electrodes was described, and used to demonstrate three μmechanical resonator devices that utilized lateral mode operation to achieve unprecedented frequency, Q, and thermal stability performances. Although already impressive, these demonstrations actually only scratch the surface of a plethora of potential performance enhancements for capacitively transduced micromechanical signal processors now made plausible via the introduction of this process. Some examples include μmechanical filters with bridging to affect loss poles, fully-integrated thermally stable μmechanical resonator reference oscillators, and μmechanical front-ends to communication receivers.

Acknowledgments: This work was supported by DARPA under Agreement No. F30602-97-2-0101.

References

[1] C. T.-C. Nguyen, "Freq.-selective MEMS for miniaturized low-power comm. devices (invited)," *IEEE Trans. Microwave Theory Tech*., vol. 47, no. 8, pp. 1486-1503, Aug. 1999.

[2] T. A. Core, W. K. Tsang, S. J. Sherman, "Fabrication technology for an integrated surface-micromachined sensor," *Solid State Technology*, pp. 39-47, Oct. 1993.

[3] K. Wang, A.-C. Wong, and C. T.-C. Nguyen, "VHF free-free beam high-Q μmechanical resonators," *IEEE/ASME J. Microelectromech. Syst*., vol. 9, no. 3, pp. 347-360, Sept. 2000.

[4] K. Wang and C. T.-C. Nguyen, "High-order medium frequency micromechanical electronic filters," *IEEE/ASME J. Microelectromech. Syst*., vol. 8, no. 4, pp. 534-557, Dec. 1999.

[5] A.-C. Wong, J. R. Clark, and C. T.-C. Nguyen, "Anneal-activated, tunable, 68MHz micromechanical filters" *Digest of Technical Papers*, 10th Int. Conference on Solid-State Sensors and Actuators, Sendai, Japan, June 7-10, 1999, pp. 1390-1393.

[6] J. R. Clark, W.-T. Hsu, and C. T.-C. Nguyen, "High-Q VHF micromechanical contour-mode disk resonators," to be published in the *Tech. Dig.*of the IEEE IEDM'00.

[7] W.-T. Hsu, J. R. Clark, and C. T.-C. Nguyen, "Mechanically temperature compensated flexural-mode μmechanical resonators," to be published in the *Tech. Dig.* of the IEEE IEDM'00.